INFECTION AND IMMUNITY, Feb. 2005, p. 1129–1140 Vol. 73, No. 2
0019-9567/05/$08.00+0 doi:10.1128/IAI.73.2.1129–1140.2005

A549 Lung Epithelial Cells Grown as Three-Dimensional Aggregates: Alternative Tissue Culture Model for *Pseudomonas aeruginosa* Pathogenesis

A. J. Carterson,[1,2] K. Höner zu Bentrup,[1] C. M. Ott,[3] M. S. Clarke,[4]† D. L. Pierson,[5] C. R. Vanderburg,[6] K. L. Buchanan,[1] C. A. Nickerson,[1] and M. J. Schurr[1,2]*

Department of Microbiology and Immunology, Program in Molecular Pathogenesis and Immunity, Tulane Center of Excellence in Bioengineering, Tulane University Health Sciences Center,[1] and Louisiana Center for Lung Biology and Immunotherapy,[2] New Orleans, Louisiana; EASI/Wyle Laboratories,[3] Division of Space Life Sciences, Universities Space Research Association,[4] and Habitability and Environmental Factors Office, NASA Johnson Space Center,[5] Houston, Texas; and Massachusetts General Hospital, Boston, Massachusetts[6]

Received 12 July 2004/Returned for modification 24 August 2004/Accepted 8 October 2004

A three-dimensional (3-D) lung aggregate model was developed from A549 human lung epithelial cells by using a rotating-wall vessel bioreactor to study the interactions between *Pseudomonas aeruginosa* and lung epithelial cells. The suitability of the 3-D aggregates as an infection model was examined by immunohistochemistry, adherence and invasion assays, scanning electron microscopy, and cytokine and mucoglycoprotein production. Immunohistochemical characterization of the 3-D A549 aggregates showed increased expression of epithelial cell-specific markers and decreased expression of cancer-specific markers compared to their monolayer counterparts. Immunohistochemistry of junctional markers on A549 3-D cells revealed that these cells formed tight junctions and polarity, in contrast to the cells grown as monolayers. Additionally, the 3-D aggregates stained positively for the production of mucoglycoprotein while the monolayers showed no indication of staining. Moreover, mucin-specific antibodies to MUC1 and MUC5A bound with greater affinity to 3-D aggregates than to the monolayers. *P. aeruginosa* attached to and penetrated A549 monolayers significantly more than the same cells grown as 3-D aggregates. Scanning electron microscopy of A549 cells grown as monolayers and 3-D aggregates infected with *P. aeruginosa* showed that monolayers detached from the surface of the culture plate postinfection, in contrast to the 3-D aggregates, which remained attached to the microcarrier beads. In response to infection, proinflammatory cytokine levels were elevated for the 3-D A549 aggregates compared to monolayer controls. These findings suggest that A549 lung cells grown as 3-D aggregates may represent a more physiologically relevant model to examine the interactions between *P. aeruginosa* and the lung epithelium during infection.

Cell culture models have been widely used to study the infectious process of *Pseudomonas aeruginosa.* The most frequently used in vitro model of lung epithelia is the monolayer, where cells are grown on flat plastic surfaces. While this system has provided important insight into the fundamentals of host-pathogen interactions, it is not without limitations. Studies show that when cells are removed from their host tissue and grown as monolayers on impermeable surfaces, they undergo dedifferentiation and lose specialized functions (13). This is thought to be, in part, the result of the disassociation of cells from their native three-dimensional (3-D) tissue structure in vivo to their two-dimensional propagation as monolayers on plastic surfaces (13, 43). Given the inherent limitations of conventional monolayers, the availability of models preserving properties of in vivo tissues that are easily manipulated would benefit the exploration of host-pathogen interactions.

The rotating-wall vessel (RWV) bioreactor (Fig. 1) is an optimized suspension cell culture technology designed for growing 3-D cells under conditions that promote many of the specialized features of in vivo tissues (16, 38, 43). The principal design feature of the RWV bioreactor is a horizontally rotating vessel that is completely filled with culture medium. As the vessel rotates, both the wall and the fluid mass rotate at the same angular rate, i.e., as a solid body. The sedimentation of the cells within the vessel is offset by the rotating fluid, creating a constant free-fall of the cells through the culture medium. Because the cells are maintained in a gentle fluid orbit, cells grown in the RWV are able to attach to one another, form the fragile connections required for complex 3-D structures, and attain a more "tissue-like" phenotype. Thus, unlike cell and tissue cultures grown in 2-D monolayers, cells cultured in the RWV bioreactor are more structurally and functionally similar to in vivo cells and tissues. Moreover, due to its low-shear/turbulence operation, the RWV reactor minimizes mechanical cell damage and thus largely solves the challenges of suspension culture: to suspend cells and microcarriers without inducing turbulence, or large degrees of shear, while providing adequate nutrition and oxygenation (15, 16, 28).

Nickerson et al. used the RWV reactor to generate high-fidelity 3-D cultures of human intestinal epithelial cells as a

* Corresponding author. Mailing address: Department of Microbiology and Immunology, Program in Molecular Pathogenesis and Immunity, Tulane University Health Sciences Center, 1430 Tulane Ave., New Orleans, LA 70112. Phone: (504) 988-4607. Fax: (504) 588-5144. E-mail: mschurr@tulane.edu.

† Present address: Laboratory of Integrated Physiology, Health and Human Performance, University of Houston, Houston, TX 77204-6015.

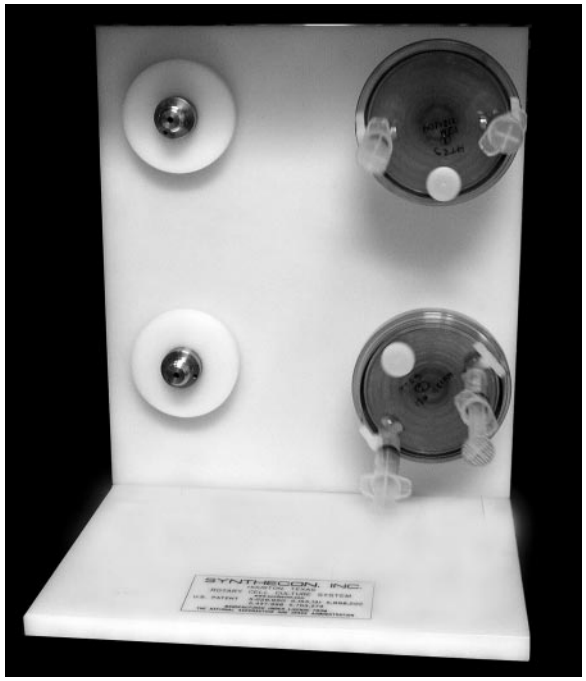

FIG. 1. RWV bioreactor. The cylindrical cell culture chamber is filled with growth medium, to which A549 cells are added. All bubbles are removed by using 5-ml syringes, and the culture chamber is attached to a base, which allows rotation of the chamber along the horizontal axis (power supply not shown). As the vessel rotates, both the wall and fluid mass rotate as a solid body. The sedimentation of the cells is offset by the rotating fluid, which creates a state of constant free fall of the cells in the growth medium. As the size of the aggregates increases, the speed of rotation is increased in compensation to maintain free fall of the aggregates in the medium. Oxygen and carbon dioxide exchange occurs through a gas-permeable silicone rubber membrane in the back of the chamber. The base shown is capable of maintaining four RWV bioreactors simultaneously (two RWV reactors with 5-ml syringes are shown attached to the base on the right-hand side).

model system to study the infectivity of the enterobacterial pathogen *Salmonella enterica* serovar Typhimurium (27). These investigations showed that 3-D cells more closely modeled in vivo parental tissue than did conventional monolayer cultures of the same cells. In response to infection with *S. enterica* serovar Typhimurium, important differences were observed between the 3-D cells and the same cells grown as monolayers, including differences in tissue pathology, adherence, invasion, apoptosis, and expression of cytokines (27). Many of these differences appeared to be more reflective of an in vivo infection (27). We have chosen to expand these studies into a lung cell model by using the A549 cell line because it has been widely used in studying *P. aeruginosa* pathogenesis (2, 8, 17, 29, 47). Moreover, when A549 cells are cultured as monolayers, they do not retain the structural or functional characteristic of the tissue from which they were derived (3, 46). Together, these characteristics of the A549 cell line make it a good candidate for RWV growth to enhance their physiological relevance in pathogenesis studies. Here, the RWV bioreactor was utilized, in conjunction with cultivation of 3-D aggregates of A549 lung epithelial cells, to explore the possibility that the low-shear culture environment in the RWV reactor may produce a differentiated cell culture model more capable of replicating an in vivo *P. aeruginosa* lung infection.

MATERIALS AND METHODS

Bacterial strains and growth conditions. All infectivity studies were performed using *P. aeruginosa* strain PAO1 (18). Bacterial cells were grown in Luria-Bertani broth at 37°C with aeration to an optical density at 600 nm of 0.4, corresponding to the mid-log growth phase. Unless otherwise stated, all studies were performed at a multiplicity of infection of 10:1.

3-D A549 cell culture methods. The human tumorigenic lung epithelial cell line A549 was obtained from the American Type Culture Collection (CCL-185). A549 cells to be cultured in three dimensions were initially grown in Corning T75 cell culture flasks containing GTSF-2 (HyClone) (22) supplemented with 10% fetal bovine serum and 100 μg of penicillin-streptomycin (Invitrogen) per ml at 37°C in 5% CO_2 before being seeded into the RWV bioreactor. On reaching 75% confluency, the A549 cells were washed with phosphate-buffered saline (PBS) and then removed from the flask by the addition of 0.25% trypsin and washed twice with PBS. Approximately 5×10^6 cells were then resuspended in fresh GTSF-2 containing 5 mg of Cytodex-3 microcarrier beads (Sigma) per ml; these are type I collagen-coated dextran beads (average diameter, 175 μm). The cells and beads were incubated together for 30 min at room temperature to allow for attachment before being placed into the RWV (Synthecon, Inc.) and cultured in GTSF-2 as previously reported (27). For all studies, except where noted, the 3-D aggregates were cultured in the RWV reactor for 12 to 14 days; then, on the day of the experiments, they were seeded on 24-well plates and fresh medium was added. A549 control monolayers were cultured in 24-well plates to 75% confluency (2 to 3 days) in GTSF-2 at 37°C under 5% CO_2.

Cell viability analysis. A549 3-D aggregates were cultured for 1, 2, or 4 weeks in the RWV reactor, while monolayer controls were grown to 75% confluency. The A549 3-D aggregates were dissociated into individual cells by treatment with 0.25% trypsin and then passed through a 104-μm stainless steel cell dissociation sieve (Sigma) to remove the carrier beads. The monolayers were released with 0.25% trypsin. The A549 monolayers and 3-D aggregates were aliquoted into separate tubes and stained with fluorescein isothiocyanate FITC-conjugated annexin V, propidium iodide, or FITC-conjugated annexin V and propidium iodide (R&D Systems) as specified by the manufacturer. The cells underwent analysis on a FACSCaliber flow cytometer (Becton Dickson) for apoptosis and cell death.

Immunohistochemistry and Alcian Blue staining. A549 cells cultured as 3-D aggregates or as monolayers were subjected to immunohistochemical characterization. For epifluorescence imaging, samples were rinsed twice with PBS solution containing 1 mM $MgCl_2$ and 1 mM $CaCl_2$ (DPBS) and then fixed with 4% formaldehyde (methanol free; Ted Pella, Inc., Redding, Calif.) in PBS for 30 min. Free aldehydes were quenched with 50 mM NH_4Cl in PBS for 10 min. The fixed cells were then permeabilized in 0.1% Triton X-100 in PBS for 5 min before nonspecific antigens were blocked for 60 min in 8% heat-inactivated goat serum. Samples were incubated overnight at 4°C with the primary antibodies ZO-1 (BD Transduction, San Diego, Calif.), occludin (a gift from J. S. Alexander, Louisian State University, Shreveport, La.), E-cadherin (Chemicon, Temecula, Calif.), β-catenin (Chemicon), MUC1 (Biomeda, Palatine, Ill.), MUC5AC (Biomeda), type IV collagen (Biodesign, Saco, Maine), and laminin β1 (Biomeda) diluted 1:50 in blocking solution, followed by secondary antibodies conjugated to Alexa-Fluor 488 or − 568 (Molecular Probes, Eugene, Oreg.). Counterstaining was performed with 4′,6-diamidino-2-phenylindole hydrochloride (DAPI). Samples were mounted in antifade solution (Molecular Probes). Epifluorescent images were acquired with a Zeiss Axioplan II microscope. Series of horizontal optical sections (0.3 μm each) were collected and subsequently deconvolved by using Slidebook 3.0 software (Intelligent Imaging Innovations, Denver, Colo.). Images represent a merging of sections spanning the apical region of A549 cells (for junctional markers and MUC1) or the basolateral region (for collagen IV and laminin) and are presented at a magnification of ×630. 630×. They are representative of several experiments.

A549 3-D aggregates and monolayer controls characterized for the tumorigenic markers, pan-keratin (Boehringer, Indianapolis, Ind.), cytokeratin 7 (NovaCastra, Newcastle upon Tyne, United Kingdom), and vimentin (DSHB, Iowa City, Iowa). were imaged by confocal microscopy as previously described (27). The concentrations of the antibodies were each 2.5 μg/ml. Confocal imaging was performed using a Zeiss LSM 400 series laser-scanning microscope. Fluorochrome excitation of Alexa 488-labeled secondary antibodies was by 488-nm filtered emission from a Kr-Ar laser source. Each image is the compilation of 16 scans of 2 s each, collected at identical exposure levels.

In addition, for the analysis of mucoglycoprotein production, A549 3-D ag-

gregates and monolayer controls were paraffin embedded, sectioned, and stained with Alcian Blue in preparation for analysis by light microscopy.

SEM. For scanning electron microscopy (SEM) analysis, 3-D cell aggregates and monolayer samples were infected with *P. aeruginosa* for either 1, 3, or 6 h and subsequently fixed in SEM fixative (3% glutaraldehyde plus 0.5% paraformaldehyde in PBS [pH 7.2]). After a minimum of 24 h of fixation, the samples were flushed in triplicate with filter-sterilized deionized water to remove salts and transferred for observation in a Philips XL 30 ESEM instrument (FEI Co., Hillsboro, Oreg.). The chamber pressure was adjusted between 1 and 2 Torr to optimize image quality.

Adherence and invasion analysis. *P. aeruginosa* adherence and invasion into A549 3-D aggregates and monolayer controls was assessed by a standard gentamicin exclusion assay as previously described (12) with the following modifications. *P. aeruginosa* was incubated with either the A549 3-D aggregates or monolayer controls in 24-well plates for 1 or 2 h. Trypan blue dye exclusion determined the average number of viable cells per well, and this was used to achieve the average multiplicity of infection of 10:1. After 1 h, the A549 cells were washed twice with PBS and lysed with 0.1% sodium deoxycholate to determine the number of bacteria adhered to the A549 cell surface. At the 1-h time point, the GTSF-2 medium in the samples to be assayed for invasion was replaced with fresh GTSF-2 medium containing 50 μg of gentamicin per ml. After 2 h the A549 cells were lysed with 0.1% sodium deoxycholate to determine the number of bacteria that had invaded. Bacterial counts were determined by serial dilution of three different wells, and the bacteria were plated onto Luria-Bertani agar. After 16 h, the CFU/per milliliter was determined. All experiments were replicated in triplicate.

Analysis of cytokine expression. A549 3-D aggregates and monolayer controls were infected for 6 h with *P. aeruginosa*, and their cytokine expression profiles were analyzed via a cytometric bead array (CBA) (BD Biosciences). Both the 3-D aggregates and monolayer controls were infected; supernatants were collected from three wells, pooled, and processed as specified by the manufacturer for each time point. Cytokine expression was analyzed on a FACSCaliber flow cytometer. All experiments were performed in triplicate from independent batches of A549 3-D aggregates and monolayers. As a control for discrepancies in numbers of cells, the A549 3-D aggregate and monolayer cells were normalized by lysis with 0.1% sodium deoxycholate, and the total protein was quantified by the Bradford assay. The amounts of cytokines produced by each sample were normalized to the amount of total protein in that sample. Fold induction was determined by dividing the amounts of cytokine produced in infected cells by the amount of cytokine produced in uninfected cells.

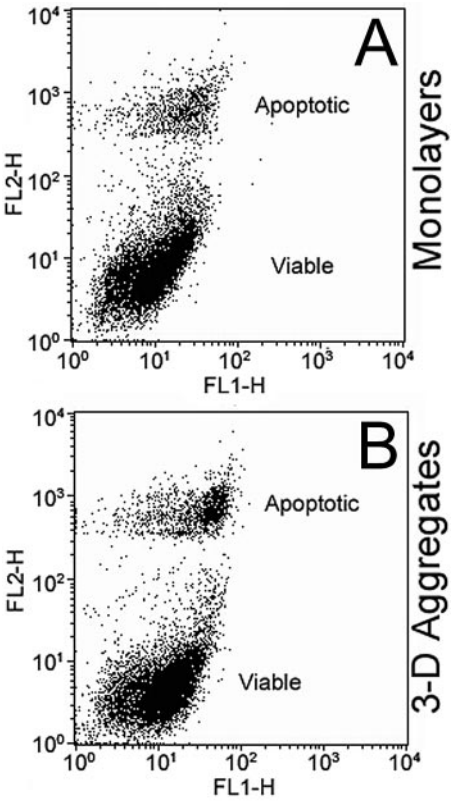

FIG. 2. A549 3-D aggregates displayed no loss of viability after a 2-week incubation in the RWV bioreactor. A549 3-D aggregates were stained for determination of the optimal growth conditions in the RWV bioreactors, such that there was aggregate formation without a loss of cell viability. The cells were disassociated with 0.25% trypsin, washed, and stained with Annexin V and propidium iodide and then underwent flow cytometry. Monolayers (A) were 86% viable, and 3-D aggregates (B) were 84% viable.

RESULTS

Growth of A549 lung epithelial cells in the RWV bioreactor. The optimal incubation period necessary to maximize 3-D aggregate formation while maintaining high cell viability was determined for A549 cells in the RWV bioreactor. Initially, A549 cells were cultured in the RWV reactor for 1, 2, or 4 weeks and compared to monolayer controls to determine a period of maximal growth and viability. Cells grown for 1 week did not form aggregates of sufficient size to be used for further examination. Likewise, cells that were incubated for 4 weeks showed a significant decrease in viability (data not shown). Cells grown for 2 weeks in the RWV reactor exhibited adequate aggregate formation and retained approximately 84% viability compared with 86% for the monolayer controls grown for 2 to 3 days (Fig. 2). A 2-week incubation period for the A549 lung epithelium cells in the RWV reactor provided optimal 3-D aggregate formation without compromising the viability of the cells, and the 3-D aggregates grown for this period were utilized for the rest of the studies.

A549 3-D aggregates display an upregulation of junctional markers. We examined the state of differentiation of the A549 3-D aggregates compared to that of the same cells grown as monolayers with respect to junctional integrity (Fig. 3). Cells were stained with four different antibodies to markers indicative of junction formation: ZO-1, occludin, E-cadherin, and β-catenin (40). In confluent A549 monolayers, the ZO-1 transmembrane protein was expressed at cell-cell contacts (Fig. 3B). However, 3-D cells clearly showed organization of ZO-1 that formed continuous circumferential zones of contact between adjacent cells, indicative of differentiated and polarized cells (Fig. 3A). The tight-junctional component occludin showed significant differences between the two cultures. Most 3-D cells expressed occludin at cell-cell borders, the distribution anticipated for normal differentiated epithelial cells (Fig. 3C). By comparison, in A549 monolayer cultures, occludin was weakly expressed in cell membranes (Fig. 3D).

E-cadherin plays a crucial role in the maintenance of the epithelial junctional complex and, as such, is important in maintaining epithelial integrity (14, 41). This marker is very densely and discretely expressed at junctional complexes in 3-D cells since it is localized in or along the cell-cell contacts similar to differentiated epithelial cells in vivo (Fig. 3E). In contrast, the A549 monolayer E-cadherin only marginally localized to cell-cell interfaces, with the majority of expression occurring throughout the cytoplasm (Fig. 3F), unlike the 3-D cells, where expression was limited to the cell-cell interface (Fig. 3E). The junctional linker protein β-catenin participates in the cadherin-β–α-catenin–cytoskeleton complex (45), and showed weak junctional organization, with nuclear association

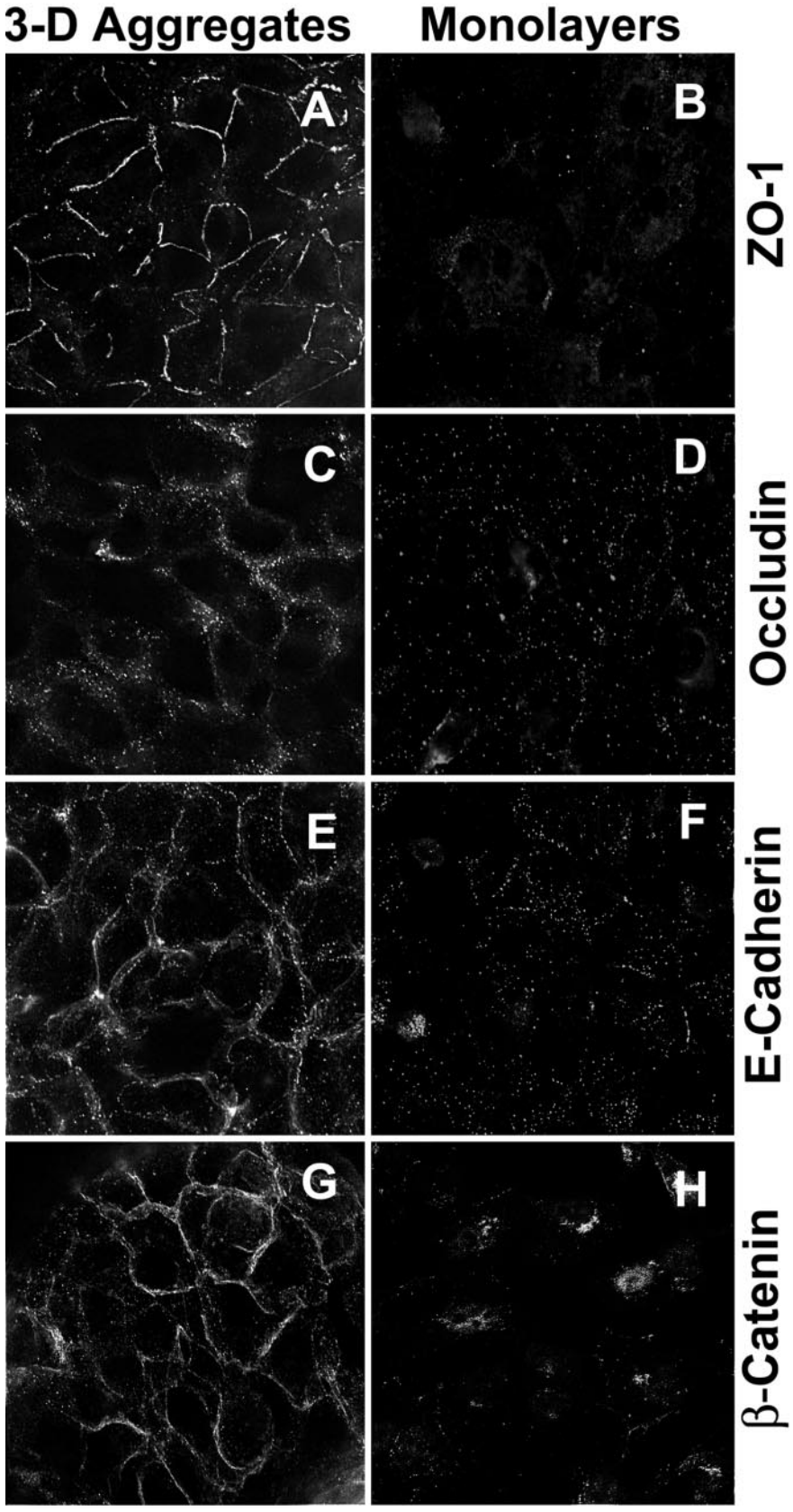

FIG. 3. A549 3-D aggregates displayed greater staining of junctional differentiation markers than did to A549 monolayer controls. A549 3-D aggregates (A, C, E, and G) and A549 monolayers (B, D, F, and H) were fixed and stained with antibodies against ZO-1 (A and B), occludin (C and D), E-cadherin (E and F), and β-catenin (G and H). 3-D aggregates showed more staining with distinct localization to the cell-cell interfaces, while monolayers had a diffuse pattern of staining.

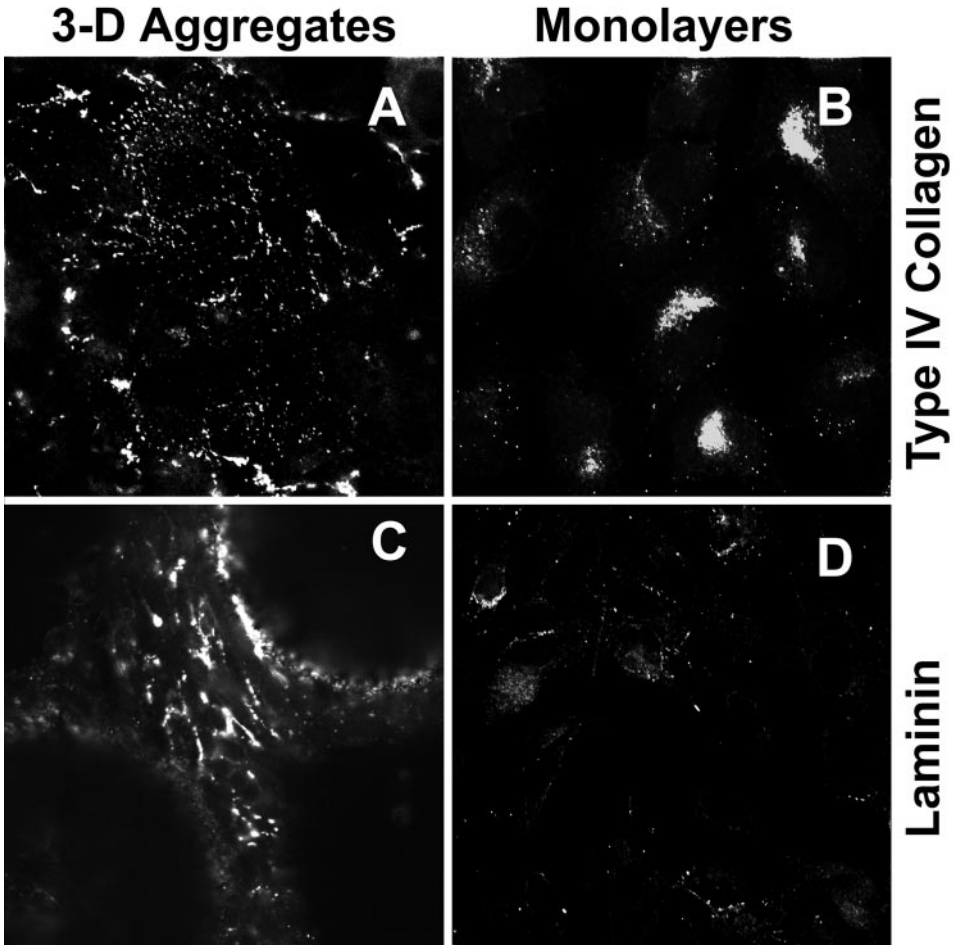

FIG. 4. A549 3-D aggregates displayed greater staining toward markers indicative of polarity. A549 3-D aggregates and monolayers were analyzed by immunohistochemistry for two markers of epithelial polarity, type IV collagen and laminin. The 3-D aggregates displayed greater staining for both type IV collagen (A) and laminin (C) at their basolateral surface than did monolayers (B and D, respectively).

within A549 cells cultured as monolayers (Fig. 3H). However, this marker was more highly enriched within the junctions of the 3-D cultured cells (Figs. 3G). These results suggest that 3-D A549 cells may form highly organized junctions, leading to better barrier integrity than in the same cells cultured as monolayers.

A549 3-D aggregates displayed greater staining of markers for epithelial polarity, type IV collagen, and laminin. The extracellular matrix protein type IV collagen is the main component of the basement membrane (7). Cells cultured as 3-D aggregates revealed a localization pattern consistent with an extracellular accumulation of this protein, while in A549 monolayers, collagen IV appeared to be retained to the perinuclear space (Fig. 4A and B, respectively). The organization of collagen IV production in 3-D cells indicated a polar, more differentiated phenotype in 3-D than in monolayer culture.

Similarly, laminin is responsible for the necessary stimulus for proper cell adhesion (30). In the 3-D aggregates, laminin was isolated to the basolateral surface and was localized to the perimeter of the cells (Fig. 4C). The A549 monolayers stained poorly with the antilaminin antibody, thereby suggesting a lack of expression when A549 cells are cultured as monolayers (Fig. 4D).

A549 3-D aggregates exhibited characteristic extracellular differentiation markers including mucin glycoproteins, MUC1 and MUC5AC. The A549 3-D aggregates and monolayer controls were stained with Alcian Blue, and immunohistochemistry was performed to detect the presence of mucopolysaccharides (Fig. 5). The A549 3-D aggregates stained positive for Alcian Blue, thereby indicating the presence of mucopolysaccharides (Fig. 5A). However, staining of the A549 monolayer controls revealed no staining for Alcian Blue, suggesting a lack of production of mucopolysaccharides (Fig. 5B).

To further characterize the production of mucins by the A549 cells grown as 3-D aggregates, both the 3-D aggregates and monolayer controls were stained with antibodies to MUC1 and MUC5AC. The MUC1 gene product is a cell-associated glycoprotein expressed on the apical surface of most normal secretory epithelia. The precise function of this protein is not well understood, although it is probable that its apical localization is important for its function. In A549 monolayers, MUC1 appeared to be entirely nucleus associated, in contrast to 3-D cultures, where immunostaining clearly showed segregation of the label to the apical domain of these cells (Fig. 5D and C, respectively). The MUC5AC gene codes for a secreted

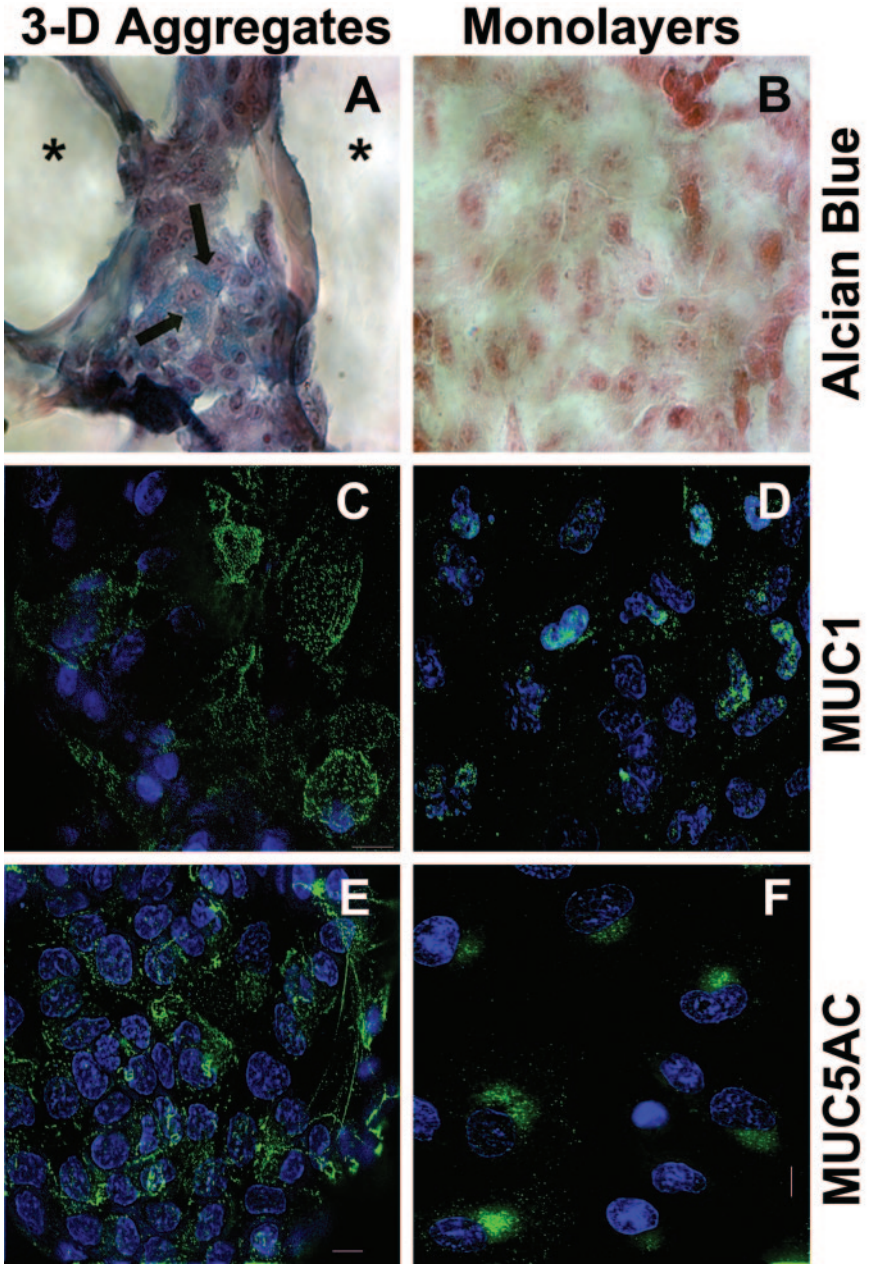

FIG. 5. 3-D A549 aggregates showed mucoglycoprotein production by Alcian Blue staining and immunohistochemistry. A549 lung epithelium grown as 3-D aggregates produce mucoglycoproteins (A), unlike their monolayer counterparts (B), as indicated by Alcian Blue staining. Moreover, the A549 3-D aggregates displayed greater staining for both MUC1 and MUC5AC (C and E), showing localization to the apical surface. However, the A549 monolayers only marginally stained for MUC1 and MUC5AC (D and F), with the stain concentrating in the perinuclear region. Taken together, these results indicate the production of the differentiation marker, mucin, by the 3-D aggregates and not by the monolayer controls. Arrows indicate mucoglycoprotein-producing cells. Asterisks indicate Cytodex-3 carrier beads.

gel-forming mucin containing cysteine-rich domains and is generally detected in goblet or goblet-like cells (42). Growth of the A549 cells as 3-D aggregates exhibited a staining pattern of MUC5AC that is indicative of an apically secreted mucin (Fig. 5E). On the other hand, monolayers revealed low-level perinuclear expression of MUC5AC (Fig. 5F).

A549 3-D aggregates displayed a reduced staining for cancer-specific markers. The A549 3-D aggregates exhibited decreased expression of the carcinoma markers pan-keratin, cytokeratin 7, and vimentin (Fig. 6). The A549 monolayer cells (Fig. 6B) showed more intense staining with anti-pan-keratin antibodies than did the 3-D aggregates (Fig. 6A), indicating a reduction of keratin isoforms in the 3-D culture. Abnormal cytokeratin 7 expression is used to identify lung adenocarcinoma (21), and staining appeared greater in the monolayer cells than the 3-D aggregates for this marker (Fig. 6C and D, respectively). Additionally, A549 3-D aggregates appeared to contain less vimentin (Fig. 6E and F, respectively). The 3-D

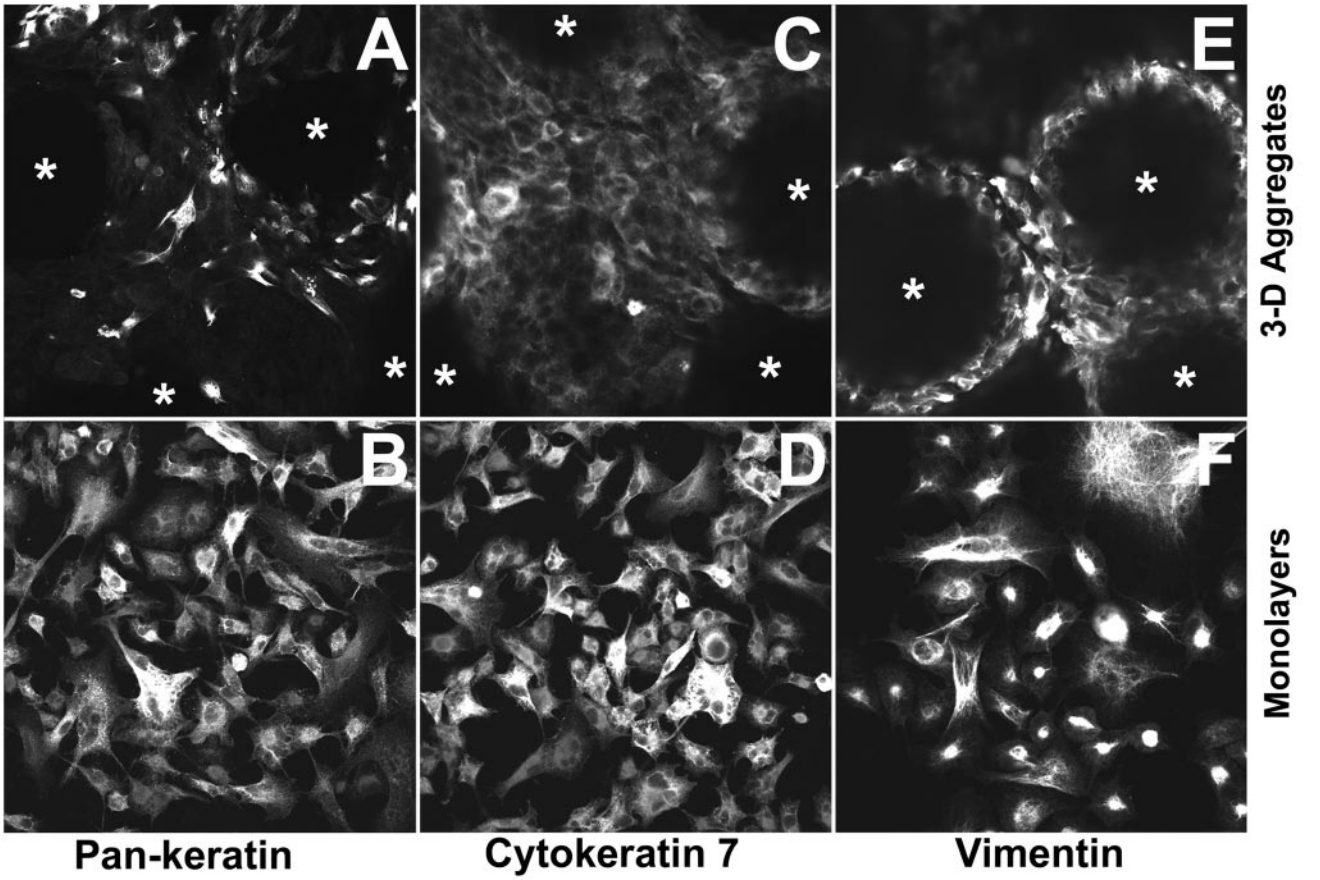

FIG. 6. A549 3-D aggregates displayed reduced staining of cancer-specific markers compared to A549 monolayer controls. A549 3-D aggregates (A, C, and E) and A549 monolayers (B, D, and F) were fixed and stained with antibodies against pan-keratin (A and B), cytokeratin 7 (C and D), and vimentin (E and F). The 3-D aggregates showed a reduced expression of these cancer stains toward cancerous markers compared to monolayers. Asterisks indicate Cytodex-3 carrier beads.

aggregates had a distinct pattern of vimentin and cytokeratin 7 localization to the outer edges of the cells, while the antibodies for both detected these proteins throughout the cytoplasm of the monolayers. Taken together, these results indicate that the 3-D aggregates decrease the amounts of cancer-specific cell markers and properly localize them, suggesting an in vivo-like physiology.

***P. aeruginosa* bound to and penetrated A549 monolayer cells more efficiently than A549 3-D aggregates.** To compare the response of A549 3-D aggregates and monolayers to *P. aeruginosa* infection, a standard gentamicin exclusion assay was used to determine the numbers of bacteria that adhered to and invaded the cells (Fig. 7A and B, respectively). Approximately 19-fold more bacteria adhered to the A549 cells grown as monolayers compared to the same cells grown as 3-D aggregates. Moreover, 40-fold more bacteria penetrated the monolayers than penetrated the 3-D aggregates. Taken together, the adherence and invasion assays indicate that *P. aeruginosa* PAO1 readily adhered to and penetrated the A549 monolayers but not the A549 3-D aggregates.

Additionally, we examined the ultrastructural morphology of the A549 3-D aggregates and monolayers after *P. aeruginosa* challenge. The cells were visualized using SEM at 0, 3, or 6 h post-challenge (Fig. 8). Both A549 monolayers and 3-D aggregates appear normal before infection (Fig. 8A and B, respectively). However, after 3 h following the *P. aeruginosa* challenge, cells within the A549 monolayers rounded and detached from the plastic surface (Fig. 8C). The A549 3-D aggregates also appeared to be undergoing morphological changes, but these were in the form of mild blebbing of the plasma membrane (Fig. 8D). By 6 h postinfection, the majority of the A549 monolayer cells exhibited rounding and detachment, while the 3-D aggregates showed more severe blebbing of the plasma membrane (Fig. 8E and F, respectively). On greater magnification after 6 h, the surface of the A549 3-D aggregates appeared pocked and severely damaged, to the extent that it appeared there were "holes" in the plasma membrane (Fig. 8H), yet the monolayer control exhibited no such damage (Fig. 8G).

A549 3-D aggregates showed greater fold induction of IL-12, TNF-α, IL-10, and IL-6 than did monolayers after *P. aeruginosa* infection. To determine the effects of *P. aeruginosa* infection on the 3-D aggregates and monolayers, a cytokine profile of the A549 3-D aggregates and A549 monolayers was determined by a CBA to quantify the interleukin-12 (IL-12), tumor necrosis factor alpha (TNF-α), IL-10, IL-6, IL-1β, and IL-8 produced (Fig. 9). At 6 h postinfection, there was a greater induction of IL-12, TNF-α, IL-10, and IL-6 in the A549 3-D aggregates than in the monolayer controls. However, the fold

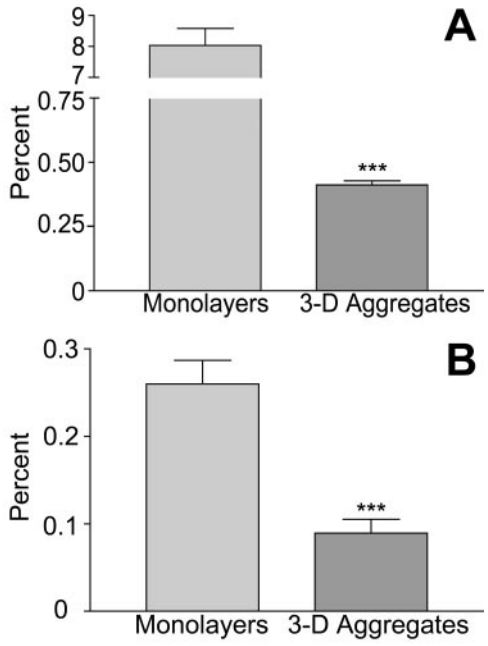

FIG. 7. *P. aeruginosa* readily bound to and penetrated the A549 monolayer cells but not the A549 3-D aggregates. (A) *P. aeruginosa* bound to the A549 monolayers 19-fold more than to the 3-D A549 aggregates when examined as a percentage of the total bacteria adhered. (B) Of the bacteria that adhered, fourfold more of the adherent bacteria penetrated into the monolayers than into the 3-D aggregates. ***, $P < 0.001$ using an unpaired t test.

induction with respect to noninfected cells was increased for IL-1β in the A549 monolayers compared to the 3-D aggregates. There was no significant difference between the A549 monolayers and the 3-D aggregates with respect to IL-8 production (Fig. 9).

DISCUSSION

Interactions between bacterial pathogens and host cells are complex and numerous. While conventional tissue culture methods, such as monolayers, have allowed researchers to dissect the interplay between pathogen and host, the exact nature of these interactions is not completely understood. This is partly because dissociation of in vivo cells propagating as monolayers on flat plastic substrates in vitro causes both structural and biochemical augmentation (13). The RWV bioreactor is an optimized form of suspension culture providing a low-shear environment that minimizes mechanical cell damage and permits the generation of 3-D tissue-like assemblies modeling many aspects of in vivo human tissue (16, 38, 43). This system has produced high-fidelity 3-D cell culture models of human intestinal epithelium for use in *Salmonella* pathogenesis (27; R. Ramamurthy, K. H. zu Bentrup, C. M. Ott, S. Alexander, K. Emami, M. Nelman-Gonzalez, T. Goodwin, D. Pierson, N. R. Pellis, and C. A. Nickerson, Abstr. 104th Gen. Meet. Am. Soc. Microbiol. 2004, abstr. B-027, 2004) and viral infection studies (24, 25). Currently, a variety of 3-D cell types are under investigation for use in pathogenesis studies (28; H. M. Carvalho, J. F. Sinclair, G. Goping, L. D. Teel, and A. D. O'Brien, Abstr. 104th Gen. Meet. Am. Soc. Microbiol. 2004, abstr. B-012, 2004.; Y. C. Smith, M. Mills, and A. D. O'Brien, Abstr. 104th Gen. Meet. Am. Soc. Microbiol. 2004, abstr. B-018, 2004). In this study, A549 lung epithelial aggregates were generated specifically for the study of *P. aeruginosa* pathogenesis and shown to more closely approximate the parental tissue than did their monolayer-grown counterparts.

Time course analysis of growth conditions of A549 cells in the RWV bioreactor optimized the time frame that permitted adequate growth and aggregate formation yet maintained cell viability. After a 2-week incubation in the RWV reactor, A549 cells displayed greater than 80% viability; however, 4 weeks of culture reduced the viability of the 3-D aggregates to less than 50%. Empirical determination of cell viability and aggregate formation needs to be made for each cell type grown in the RWV bioreactor.

In polarized epithelia, specialized structures such as tight junctions and adherens junctions are responsible for the establishment of contacts between neighboring cells to ensure the separation between apical and basolateral regions of the plasma membrane. Tight junctions are a collection of proteins that regulate diffusions across the epithelium (40). Interestingly, there is evidence that A549 lung epithelial cells do not form functional tight junctions, failing to show significant immunostaining against the tight-junction protein ZO-1 (46). However, there was diffuse, nonlocalized expression of the tight-junction protein occludin by the A549 monolayers. More importantly, the A549 3-D aggregates displayed significant immunostaining against ZO-1 that localized to the cell-cell interface. The 3-D aggregates expressed occludin, another tight-junction protein, on the outer periphery of the cells, indicating proper localization to the points of cell contact between neighboring cells.

Cadherins are a family of proteins that mediate cell-cell interactions between neighboring epithelioid cells, via adherens junctions, usually in a calcium-dependent manner (9). E-cadherin is thought to be an important component of the signaling cascade between the cell and the extracellular milieu by linking to the actin cytoskeleton via several submembrane proteins, including β-catenin (14, 45). Studies of cancer cell lines have shown that changes in the structure or expression of the components of the E-cadherin/β-catenin complex result in suppression of the cell-cell adhesion and in expression of an invasive phenotype (41). The 3-D aggregates avidly expressed both E-cadherin and β-catenin to the outer edges of the cells wherever the cells made contact with neighboring cells. However, the monolayers had irregular and sporadic localization of E-cadherin and β-catenin. Together, immunohistochemistry results for tight and adherens junctions suggest that RWV cultivation allows A549 3-D aggregates to form more in vivo-like junctional complexes.

The basement membrane constituents, including type IV collagen and laminin, are basolateral proteins essential in providing the scaffolding and support necessary for polarity in functional tissues (7). Collagens are the primary structural proteins that help give the basement membrane its stability, with type IV being the most important in barrier epithelia. Therefore, we examined the localization of type IV collagen in the A549 3-D aggregates and monolayer cells. Evidence of type IV collagen production was seen in both the 3-D aggregates and the monolayers; however, there was a marked distinction in localization. The 3-D aggregates displayed localization to

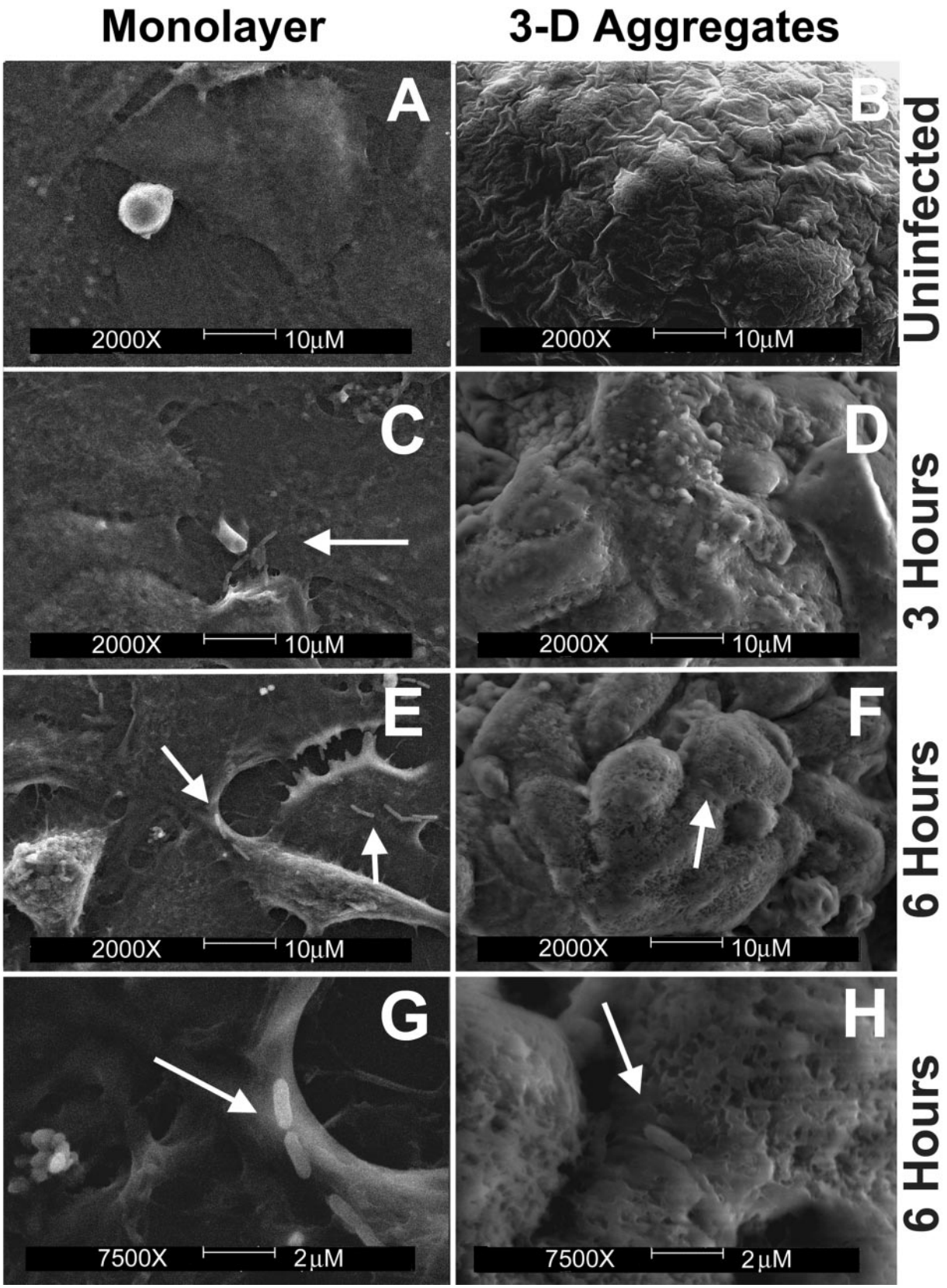

FIG. 8. *P. aeruginosa* infection damaged the cellular surface of A549 3-D aggregates but caused rounding and detachment of A549 Monolayers. Images were taken of uninfected monolayers and 3-D aggregates (A and B, respectively), 3 h after infection with *P. aeruginosa* (C and D, respectively), 6 h postinfection (E and F, respectively), and 6 h postinfection at a higher magnification (G and H, respectively). While 3-D aggregates appear to be causing greater damage to their plasma membrane, they do not round and detach from the substrate as the monolayer control does.

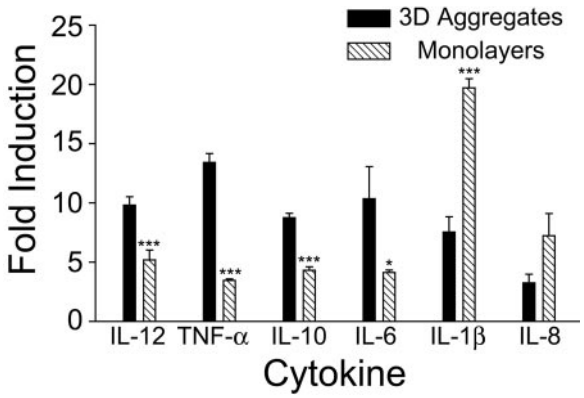

FIG. 9. A549 3-D aggregates exhibited a greater induction in the cytokines IL-12p70, TNF-α, IL-10 and IL-6 than did A549 monolayers. The result of CBA analysis of cytokine production in A549 3-D aggregates and monolayers at 6 h after infection with *P. aeruginosa* is shown. A549 3-D aggregates exhibited greater induction of the cytokines IL-12p70, TNF-α, IL-10, and IL-6, than did to A549 monolayers. Monolayers exhibited a greater induction of IL-1β and IL-8. Supernatant was collected from three independent wells from triplicate experiments. ***, $P < 0.001$; *, $P < 0.05$ (unpaired *t* test).

the basolateral surface of the cell. However, nuclear localization of the collagen in the monolayers suggested improper synthesis. In conjunction with collagen, laminin plays an important role in the adhesion of the individual cells to the extracellular matrix, where they are known to effect cell differentiation (7). The deregulation of laminin in tumor cells leads to increased invasion and metastasis (30). Laminin production was found in the 3-D aggregates on the basolateral face, particularly where the cells contacted the microcarrier bead. However, the monolayers showed almost a complete lack of laminin after analysis by immunohistochemistry. Therefore, evidence of increased synthesis and proper localization of both type IV collagen and laminin by the 3-D aggregates denotes the establishment of polarity, further suggesting that their organization more closely resembles in vivo tissue.

Mucus is a normal constituent of lung epithelia and is composed primarily of large, heavily glycosylated proteins with sizes ranging from several hundred to thousands of kilodaltons (6, 44). Currently 13 different mucin genes (*MUC*) have been identified, with MUC2, MUC5AC and MUC5B being the primary respiratory mucins (4, 44). However, both MUC2 and MUC5B are expressed at very low levels in respiratory carcinoma cell lines such as A549 (4). Furthermore, MUC1 has been suggested as an additional adhesin for the *P. aeruginosa* protein flagellin (23, 34). There are several adhesin-receptor pairs that have been candidates for *P. aeruginosa*, but a single factor has yet to emerge; therefore, it is more likely to be a combination of various adhesins that mediate the event (1, 10, 31, 33, 35, 36). This may explain why the A549 monolayers have more adhesin while producing reduced amounts of MUC1. The 3-D aggregates, as opposed to the monolayers, stained with Alcian Blue, indicating extracellular production of mucoglycoproteins. Further investigation by immunohistochemistry revealed that the A549 3-D aggregates produced both MUC1 and the major respiratory system-associated mucin MUC5AC. Both of these proteins were found on the apical surface of the 3-D aggregates, indicating proper localization. The monolayers produced minimal amounts of both MUC1 and MUC5AC, localized to the perinuclear regions of the cells, possibly within the Golgi-endoplasmic reticulum complex. These results showed that mucin was produced extracellularly by the 3-D A549 cells and intracellularly by the monolayer-grown cells, indicating a more relevant in vivo-like expression of mucins by the 3-D aggregates.

Keratin and cytokeratin 7 were used in these immunohistochemical studies as identifiers of carcinomas, since their expression in normal tissue is a tissue-specific phenomenon (21). They form the intermediate filament proteins that are partially responsible for the structural integrity and shape of epithelial cells based on their incorporation into the cytoskeleton (9). Another carcinoma marker tested, vimentin, is also an intermediate filament protein. It mediates cell structural adherence about the basolateral surfaces and is most often associated with motile fibroblast-like phenotypes. In A549 monolayers, these markers were not localized to any specific region within the cells but instead were found throughout the cytoplasm and membrane. Conversely, the 3-D aggregates displayed downregulation or proper localization of cancer-specific markers by the 3-D aggregates, suggesting in vivo organization.

The results of adherence and invasion studies confirmed reports of what happened when a different *P. aeruginosa* strain was used to infect A549 monolayers. Chi et al. reported that *P. aeruginosa* strain PAK bound avidly to A549 monolayers and that the bacteria were internalized 2 to 3 h postinfection (8). Additionally, these investigators observed rounding and detachment of approximately 40% of the A549 epithelial cells from the plastic substrate 3 h postinfection (8). When the 3-D A549 aggregates were challenged with *P. aeruginosa* PAO1, only marginal adherence was observed and the bacteria rarely penetrated the epithelial cells. These observations are consistent with previous reports of the invasiveness of *P. aeruginosa.* Evidence obtained with Madin-Darby canine kidney cells (MDCK) (11), corneal epithelial cells (12), and the human bronchial epithelial 14o- cell line (32) suggested that *P. aeruginosa* does not invade cells with defined polarity and tight junctions. Taken together, the lack of *P. aeruginosa* PAO1 penetration and the enhanced formation of tight-junction complexes by the 3-D aggregates indicate a higher degree of differentiation.

The results of adherence, invasion, and tissue pathology studies provided insight into the pathogenic relationship between *P. aeruginosa* and A549 epithelial cells. The monolayer controls reacted differently to infection than did the 3-D aggregates. Indications of this finding included the rounding and detachment of the monolayer A549 cells from the plastic. This is in stark contrast to the 3-D aggregate response to the infection, since the 3-D aggregates remained bound to their microcarrier beads and displayed plasma membrane alterations rather than overall changes in structural morphology. The changes displayed by the 3-D aggregates included cytoskeletal changes such as blebbing and lesion formation. These structural alterations appeared to worsen over the course of the infection, but at no time did the cells physically detach from the microcarrier beads. Interestingly, few bacteria were visualized on the 3-D aggregates, and, according to the invasion assays, few were internalized. This finding is consistent with what was previously reported for *S. enterica* serovar Typhi-

murium infection of 3-D models of human small intestinal epithelium (27). Therefore, our SEM analysis supports findings from adherence assays showing that few bacteria were adhered to the 3-D aggregate cell surface. Previous findings (11, 32) asserting that junction complex formation prevented *P. aeruginosa* from penetrating into the epithelia are supported by the present work investigating the use of A549 3-D aggregates as a pathogenesis model.

Due to their actions as mediators of the host immune response, cytokines released with the onset of an infection are important host-mediated factors in deciding the direction and outcome of the disease progression (39). The establishment of a chronic *P. aeruginosa* infection in the lungs of patients with cystic fibrosis is thought to constantly restimulate the surrounding tissues to produce proinflammatory cytokines enhancing the destructive pathobiology witnessed in the lungs of patients with cystic fibrosis, presumably by the continued immune cell effector response (5, 19, 20, 37). Therefore, evaluating the differences in the cytokine profiles between the 3-D aggregates and the monolayers was particularly important to determine the usefulness of the 3-D aggregate system in pathogenesis studies. The 3-D aggregates responded to *P. aeruginosa* challenge by increasing the production of the cytokines IL-12, TNF-α, IL-10, and IL-6. It is not surprising that the 3-D aggregates, in elevating proinflammatory IL-12 levels, also exhibit induction of anti-inflammatory IL-10, thereby constituting a negative-feedback system where proinflammatory cytokines induce anti-inflammatory mediators to regulate the potentially destructive inflammatory state (26). However, more importantly, the monolayer controls do not exhibit as strong an IL-10 response as the 3-D aggregates, suggesting a weak negative-feedback mechanism. Therefore, it would appear that the cytokine profile of the 3-D aggregates could be more representative of the complex regulatory network that governs the proinflammatory cascade. This pattern of regulation is not seen in the monolayers, as evidenced by the undiminished levels of IL-1β. Together, these results indicate a level of cytokine regulation in the 3-D aggregates that more resemble the cascades found in vivo.

Our results with the A549 lung epithelial cell line grown in the RWV bioreactor were similar to those obtained by Nickerson et al. with Int-407 intestinal epithelial cells with respect to markers of epithelial cell differentiation and organization, tight-junction formation, cancer-specific markers, and cytokine production (27). Both the intestinal and lung epithelial cell lines cultured in the RWV bioreactor displayed increased expression of specific epithelial cell markers and expression of mucus. Additionally, both the 3-D intestinal and lung cell lines had decreased expression of cancer-specific cell markers. Moreover, there were significant differences in cytokine production (for the A549 cell line) and cytokine gene expression (for Int-407) between the 3-D aggregates and monolayer cultures postinfection. Taken together, the results of experiments with two independent epithelial cell lines (A549 and Int-407) indicate that the growth conditions in the RWV reactor induce in vivo-like expression of cellular contact proteins and extracellular matrix proteins and downregulate cancer-specific markers compared to the same cells grown as monolayers. Moreover, the abilities of the pathogens (*Salmonella* in the case of Int-407 cells and *Pseudomonas* in the case of A549 cells) to cause infection were more in vivo-like for the 3-D aggregates than for the monolayers in both cases. However, as with all in vitro models, limitations exist. The temporal and structural changes of cell functions such as protein expression, signaling events, and mucin production are surely all affected by RWV cultivation, but unfortunately these questions will be answered only by future extended and detailed studies. While the 3-D aggregates show similarities to in vivo tissue, they are not a replacement for actual tissue, and the model is presented as another possibility for researchers. Nevertheless, results from these studies further support the utility of the RWV bioreactor to provide physiologically relevant models of human cells and tissues for use in studying infectious disease.

ACKNOWLEDGMENTS

We thank William Uicker for lending his expertise in flow cytometry and J. S. Alexander for his generous gift of the occludin antibody.

This work was supported by the Louisiana Center for Lung Biology and Immunotherapy, grants LEQSF (1999–02) RD-A-42 and HEF (2000–05)-06 from the State of Louisiana Board of Regents (M.J.S.), National Aeronautics and Space Administration (NASA) grant NAG 2-1378 (C.A.N.), and a generous grant from the William Keck Foundation of Los Angeles, Calif.

REFERENCES

1. **Arora, S. K., B. W. Ritchings, E. C. Almira, S. Lory, and R. Ramphal.** 1998. The *Pseudomonas aeruginosa* flagellar cap protein, FliD, is responsible for mucin adhesion. Infect. Immun. **66:**1000–1007.
2. **Azghani, A. O., J. W. Baker, S. Shetty, E. J. Miller, and G. J. Bhat.** 2002. *Pseudomonas aeruginosa* elastase stimulates ERK signaling pathway and enhances IL-8 production by alveolar epithelial cells in culture. Inflamm. Res. **51:**506–510.
3. **Balis, J. U., S. D. Bumgarner, J. E. Paciga, J. F. Paterson, and S. A. Shelley.** 1984. Synthesis of lung surfactant-associated glycoproteins by A549 cells: description of an in vitro model for human type II cell dysfunction. Exp. Lung Res. **6:**197–213.
4. **Berger, J. T., J. A. Voynow, K. W. Peters, and M. C. Rose.** 1999. Respiratory carcinoma cell lines. MUC genes and glycoconjugates. Am. J. Respir. Cell Mol. Biol. **20:**500–510.
5. **Berger, M.** 2002. Inflammatory mediators in cystic fibrosis lung disease. Allergy Asthma Proc. **23:**19–25.
6. **Boat, T. F., and P. W. Cheng.** 1980. Biochemistry of airway mucus secretions. Fed. Proc. **39:**3067–3074.
7. **Bosman, F. T., and I. Stamenkovic.** 2003. Functional structure and composition of the extracellular matrix. J. Pathol. **200:**423–428.
8. **Chi, E., T. Mehl, D. Nunn, and S. Lory.** 1991. Interaction of *Pseudomonas aeruginosa* with A549 pneumocyte cells. Infect. Immun. **59:**822–828.
9. **Chothia, C., and E. Y. Jones.** 1997. The molecular structure of cell adhesion molecules. Annu. Rev. Biochem. **66:**823–862.
10. **Feldman, M., R. Bryan, S. Rajan, L. Scheffler, S. Brunnert, H. Tang, and A. Prince.** 1998. Role of flagella in pathogenesis of *Pseudomonas aeruginosa* pulmonary infection. Infect. Immun. **66:**43–51.
11. **Fleiszig, S. M., D. J. Evans, N. Do, V. Vallas, S. Shin, and K. E. Mostov.** 1997. Epithelial cell polarity affects susceptibility to *Pseudomonas aeruginosa* invasion and cytotoxicity. Infect. Immun. **65:**2861–2867.
12. **Fleiszig, S. M., T. S. Zaidi, M. J. Preston, M. Grout, D. J. Evans, and G. B. Pier.** 1996. Relationship between cytotoxicity and corneal epithelial cell invasion by clinical isolates of *Pseudomonas aeruginosa.* Infect. Immun. **64:** 2288–2294.
13. **Freshney, R. I.** 2000. Culture of animal cells: a manual of basic technique, 4th ed. Wiley-Liss, New York, N.Y.
14. **Fukata, M., and K. Kaibuchi.** 2001. Rho-family GTPases in cadherin-mediated cell-cell adhesion. Nat. Rev. Mol. Cell. Biol. **2:**887–897.
15. **Goodwin, T. J., T. L. Prewett, D. A. Wolf, and G. F. Spaulding.** 1993. Reduced shear stress: a major component in the ability of mammalian tissues to form three-dimensional assemblies in simulated microgravity. J. Cell. Biochem. **51:**301–311.
16. **Hammond, T. G., and J. M. Hammond.** 2001. Optimized suspension culture: the rotating-wall vessel. Am. J. Physiol. Ser. F **281:**F12–F25.
17. **Haussler, S., I. Ziegler, A. Lottel, F. von Gotz, M. Rohde, D. Wehmhohner, S. Saravanamuthu, B. Tummler, and I. Steinmetz.** 2003. Highly adherent small-colony variants of *Pseudomonas aeruginosa* in cystic fibrosis lung infection. J. Med. Microbiol. **52:**295–301.
18. **Holloway, B. W.** 1955. Genetic recombination in *Pseudomonas aeruginosa.* J. Gen. Microbiol. **13:**572–581.

19. **Konstan, M. W., and M. Berger.** 1997. Current understanding of the inflammatory process in cystic fibrosis: onset and etiology. Pediatr. Pulmonol. **24:** 137–142; discussion, 159–161.
20. **Kube, D., U. Sontich, D. Fletcher, and P. B. Davis.** 2001. Proinflammatory cytokine responses to *P. aeruginosa* infection in human airway epithelial cell lines. Am. J. Physiol. Ser. L **280:**L493–L502.
21. **Kummar, S., M. Fogarasi, A. Canova, A. Mota, and T. Ciesielski.** 2002. Cytokeratin 7 and 20 staining for the diagnosis of lung and colorectal adenocarcinoma. Br. J. Cancer **86:**1884–1887.
22. **Lelkes, P. I., E. Ramos, V. V. Nikolaychik, D. M. Wankowski, B. R. Unsworth, and T. J. Goodwin.** 1997. GTSF-2: a new, versatile cell culture medium for diverse normal and transformed mammalian cells. In Vitro Cell Dev. Biol. Anim. **33:**344–351.
23. **Lillehoj, E. P., B. T. Kim, and K. C. Kim.** 2002. Identification of *Pseudomonas aeruginosa* flagellin as an adhesin for Muc1 mucin. Am. J. Physiol. Ser. L **282:**L751–L756.
24. **Long, J. P., S. Pierson, and J. H. Hughes.** 1998. Rhinovirus replication in HeLa cells cultured under conditions of simulated microgravity. Aviat. Space Environ. Med. **69:**851–856.
25. **Long, J. P., S. Pierson, and J. H. Hughes.** 1999. Suppression of Epstein-Barr virus reactivation in lymphoblastoid cells cultured in simulated microgravity. In Vitro Cell. Dev. Biol. **35:**49–54.
26. **Murphy, E. E., G. Terres, S. E. Macatonia, C. S. Hsieh, J. Mattson, L. Lanier, M. Wysocka, G. Trinchieri, K. Murphy, and A. O'Garra.** 1994. B7 and interleukin 12 cooperate for proliferation and interferon gamma production by mouse T helper clones that are unresponsive to B7 costimulation. J. Exp. Med. **180:**223–231.
27. **Nickerson, C. A., T. J. Goodwin, J. Terlonge, C. M. Ott, K. L. Buchanan, W. C. Uicker, K. Emami, C. L. LeBlanc, R. Ramamurthy, M. S. Clarke, C. R. Vanderburg, T. Hammond, and D. L. Pierson.** 2001. Three-dimensional tissue assemblies: novel models for the study of *Salmonella enterica* serovar Typhimurium pathogenesis. Infect. Immun. **69:**7106–7120.
28. **Nickerson, C. A., and C. M. Ott.** 2004. A new dimension in modeling infectious disease. ASM News **70:**169–175.
29. **O'Malley, Y. Q., K. J. Reszka, G. T. Rasmussen, M. Y. Abdalla, G. M. Denning, and B. E. Britigan.** 2003. The *Pseudomonas* secretory product pyocyanin inhibits catalase activity in human lung epithelial cells. Am. J. Physiol. Ser. L **285:**L1077–L1086.
30. **Patarroyo, M., K. Tryggvason, and I. Virtanen.** 2002. Laminin isoforms in tumor invasion, angiogenesis and metastasis. Semin. Cancer Biol. **12:**197–207.
31. **Plotkowski, M. C., A. O. Costa, V. Morandi, H. S. Barbosa, H. B. Nader, S. de Bentzmann, and E. Puchelle.** 2001. Role of heparan sulphate proteoglycans as potential receptors for non-piliated *Pseudomonas aeruginosa* adherence to non-polarised airway epithelial cells. J. Med. Microbiol. **50:**183–190.
32. **Plotkowski, M. C., S. de Bentzmann, S. H. Pereira, J. M. Zahm, O. Bajolet-Laudinat, P. Roger, and E. Puchelle.** 1999. *Pseudomonas aeruginosa* internalization by human epithelial respiratory cells depends on cell differentiation, polarity, and junctional complex integrity. Am. J. Respir. Cell Mol. Biol. **20:**880–890.
33. **Prince, A.** 1992. Adhesins and receptors of *Pseudomonas aeruginosa* associated with infection of the respiratory tract. Microb. Pathog. **13:**251–260.
34. **Ramphal, R., and S. K. Arora.** 2001. Recognition of mucin components by *Pseudomonas aeruginosa.* Glycoconj. J. **18:**709–713.
35. **Ramphal, R., and G. B. Pier.** 1985. Role of *Pseudomonas aeruginosa* mucoid exopolysaccharide in adherence to tracheal cells. Infect. Immun. **47:**1–4.
36. **Ramphal, R., J. C. Sadoff, and M. Pyle.** 1984. Role of pili in the adherence of *Pseudomonas aeruginosa* to mammalain buccal epithelial cells. Infect. Immun. **44:**38–40.
37. **Rastogi, D., A. J. Ratner, and A. Prince.** 2001. Host-bacterial interactions in the initiation of inflammation. Paediatr. Respir. Rev. **2:**245–252.
38. **Schwartz, R. P., and D. A. Wolf.** June 1991. Rotating bioreactor cell culture apparatus. U.S. patent 4988623.
39. **Steinhauser, M. L., C. M. Hogaboam, S. L. Kunkel, N. W. Lukacs, R. M. Strieter, and T. J. Standiford.** 1999. IL-10 is a major mediator of sepsis-induced impairment in lung antibacterial host defense. J. Immunol. **162:** 392–399.
40. **Stevenson, B. R., and B. H. Keon.** 1998. The tight junction: morphology to molecules. Annu. Rev. Cell Dev. Biol. **14:**89–109.
41. **Takeichi, M.** 1991. Cadherin cell adhesion receptors as a morphogenetic regulator. Science **251:**1451–1455.
42. **Thornton, D. J., and J. K. Sheehan.** 2004. From mucins to mucus: toward a more coherent understanding of this essential barrier. Proc. ATS **1:**54–61.
43. **Unsworth, B. R., and P. I. Lelkes.** 1998. Growing tissues in microgravity. Nat. Med. **4:**901–907.
44. **Voynow, J. A.** 2002. What does mucin have to do with lung disease? Paediatr. Respir. Rev. **3:**98–103.
45. **Wheelock, M. J., and K. R. Johnson.** 2003. Cadherin-mediated cellular signaling. Curr. Opin. Cell Biol. **15:**509–514.
46. **Winton, H. L., H. Wan, M. B. Cannell, D. C. Gruenert, P. J. Thompson, D. R. Garrod, G. A. Stewart, and C. Robinson.** 1998. Cell lines of pulmonary and non-pulmonary origin as tools to study the effects of house dust mite proteinases on the regulation of epithelial permeability. Clin. Exp. Allergy **28:** 1273–1285.
47. **Worgall, S., K. Martushova, A. Busch, L. Lande, and R. G. Crystal.** 2002. Apoptosis induced by *Pseudomonas aeruginosa* in antigen presenting cells is diminished by genetic modification with CD40 ligand. Pediatr. Res. **52:** 636–644.

Editor: J. N. Weiser